Supplement of Atmos. Chem. Phys., 26, 349–363, 2026
https://doi.org/10.5194/acp-26-349-2026-supplement

Supplement of

Direct observation of core-shell structure and water uptake of individual submicron urban aerosol particles

Ruiqi Man et al.

Correspondence to: Zhijun Wu (zhijunwu@pku.edu.cn)

1. Calculations of optical density and its uncertainty

As mentioned in the manuscript, I is the intensity of photons transmitted through a sample region, and I_0 is the intensity of photons transmitted through a sample-free region. As shown in the following equations, the actual intensity was obtained by deducting the intensity without X-ray penetration (I_{dark}) from the measured value:

$$I = I_{meas} - I_{dark} \qquad \text{Eq. S1}$$

$$I_0 = I_{0,meas} - I_{dark} \qquad \text{Eq. S2}$$

$$I_{dark} = C_{dark} * t_d \qquad \text{Eq. S3}$$

where I_{meas} and $I_{0,meas}$ represent the intensity measured with or without sample grids. C_{dark} represents the dark counts with a unit of counts per second (cps), and t_d represents the dwell time (s). Dark counts are exactly due to noise from the detector and directly measured as the photon count rate when the X-ray beam is blocked.

Based on rules of error propagation, the uncertainty of intensity (σ_I, σ_{I0}) and optical density (OD) (σ_{OD}) were calculated as follows,

$$\sigma_I = \sqrt{I_{meas} + I_{dark}} \qquad \text{Eq. S4}$$

$$\sigma_{I0} = \sqrt{I_{0,meas} + I_{dark}} \qquad \text{Eq. S5}$$

$$\sigma_{OD} = \sqrt{\frac{I_{meas} + I_{dark}}{(I_{meas} - I_{dark})^2} + \frac{I_{0,meas} + I_{dark}}{(I_{0,meas} - I_{dark})^2}} \qquad \text{Eq. S6}$$

2. Collection and measurement of ambient particles in the environmental cell

Using ambient samples in the environmental cell had many technical challenges that we had to overcome to make this study possible. Firstly, sealing the sample and the back SiNit window requires Crystalbond 509 mounting adhesive that is applied as a fluid at 150°C and cooled to ambient temperature to form a solid vacuum tight seal. This can result in a major drawback if ambient particles are collected on the windows using field-deployed impactors and later sealed to the sample clip, subjecting them to high temperature. This may have a significant influence on chemical composition, morphology, and properties of particles[1]. A previous STXM/NEXAFS study investigated ambient particles in a humidified environmental cell tracking their water uptake, although the particles were exposed to high temperature for sealing[2]. We aimed to avoid exposing particles to high temperature, which requires presealed SiNit windows. In our attempts, we aimed to impact particles onto presealed SiNit windows in sample clips, however, the dimensions of the sample clip are quite bulky to be used in most impactor instrumentation, often making it impossible to utilize. Overall, there is a final risk to shatter the membranes that make up the SiNit windows due to physically handling samples from impactor mounting, transporting, sample sealing in clips, and mounting clips in the environmental cell and in the STXM/NEXAFS vacuum chamber.

This study has uniquely improved the original in-situ cell with a simple solution, by using continuous carbon coated copper grids to collect ambient particles and avoiding exposure to high temperature during the sealing of windows. Ambient particles are first impacted onto the grids, which are then tapped directly onto the presealed SiNit window using Kapton tape and a high vacuum silicon-based adhesive. This procedure ensured that the copper grid substrates with ambient particles were held firmly inside the environmental cell. The rest of the environmental cell, including the gas connections and operations, were identical to the original design.

3. Oxygen K-edge NEXAFS spectra of sodium chloride

Oxygen K-edge NEXAFS spectra of the sodium chloride (NaCl) standard sample obtained from six times of line scan at high RH were shown in Fig. S3. For panels (A) – (C), the RH was 75.6 ± 1.1%. For panels (D) – (F), the RH was 79.4 ± 0.8%. According to reference, the NaCl spectra generally exhibited three main features of oxygen K-edge, that is, pre-edge (~535 eV), main-edge (~537.5 eV), and post-edge (~540 eV)[3-6], clearly indicating the presence of liquid water. In our study, the main peak of NaCl spectra appeared at about 536.3 eV, and the pre-edge and post-edge were 533.8 and 538.7 eV, respectively. Compared with peaks measured in the publications, the offset of the NEXAFS spectra at the oxygen K-edge was around +1.2 eV. A small peak was observed at around 531.3 eV (532.5 eV after energy calibration), which may refer to the $1s\rightarrow\pi^*$ (e.g. from carboxyl or ketone) transitions[7], likely due to minor contamination of organic matter.

4. Calculations of the circular equivalent diameter

The circular equivalent diameter (D_{eqiv}) of an individual particle was calculated as follows,

$$D_{eqiv} = 2\sqrt{\frac{A_{ROI}}{\pi}} \qquad \text{Eq. S7}$$

where A_{ROI} is the area of the region of interest (ROI) of a particle calculated by multiplying the area of a single pixel by the total number of pixels of the ROI.

5. Estimations of oxygen-to-carbon ratio based on the STXM data

The atomic photoabsorption cross section (μ_a) with a unit of m^2 atom^{-1} can be obtained from the following relation,

$$\mu_a = 2r_0\lambda f_2 \qquad \text{Eq. S8}$$

in which r_0 is the classical electron radius in meters, λ is the wavelength of incident light in meters, f_2 is the atomic scattering factor, and it can be obtained from Henke et al. (1993)[8]. The specific values are shown in Table S1.

$$\mathrm{OD} = \mu\rho d = \mu_a n d \qquad \text{Eq. S9}$$

where ρ is the density of samples, n is the atomic density with a unit of atoms per cubic meter, and d is the thickness of samples. Therefore, we can get oxygen-to-carbon ratio (O:C, x_O/x_C) from the following equations,

$$\Delta\mathrm{OD}_c = OD_{320eV} - OD_{278eV} = \mu_{C,\,320eV} n_c d - \mu_{C,\,278eV} n_c d \qquad \text{Eq. S10}$$

$$\Delta\mathrm{OD}_O = OD_{550eV} - OD_{525eV} = \mu_{O,\,550eV} n_O d - \mu_{O,\,525eV} n_O d \qquad \text{Eq. S11}$$

$$\frac{\Delta\mathrm{OD}_C}{\Delta\mathrm{OD}_O} = \frac{n_C}{n_O} \cdot \frac{\mu_{C,\,320eV} - \mu_{C,\,278eV}}{\mu_{O,\,550eV} - \mu_{O,\,525eV}} \qquad \text{Eq. S12}$$

$$\frac{x_O}{x_C} = \frac{n_O}{n_C} = \frac{\left(\mu_{C,\,320eV} - \mu_{C,\,278eV}\right)}{\left(\mu_{O,\,550eV} - \mu_{O,\,525eV}\right)} \cdot \frac{\Delta\mathrm{OD}_O}{\Delta\mathrm{OD}_C} \qquad \text{Eq. S13}$$

Table S1. The atomic scattering factor (f_2) and corresponding atomic photoabsorption cross section (μ_a) of certain element at the pre-edge or post-edge.

Atom	Photo Energy (eV)	f_2	μ_a (m^2 atom^{-1})
Carbon (C)	278	0.1538	3.8442×10^{-24}
	320	3.626	7.8735×10^{-23}
Oxygen (O)	525	0.2394	3.1685×10^{-24}
	550	4.331	5.4716×10^{-23}

Table S 2 The data set of the oxygen-to-carbon (O:C) ratio based on AMS data using "Improved-Ambient" Methods[9] during the individual particle collection period.

Date and Time	O:C
2019/10/1 17:05	0.61
2019/10/1 17:06	0.61
2019/10/1 17:07	0.60
2019/10/1 17:08	0.59
2019/10/1 17:09	0.58

6. Calculations of the margin of error of proportions of particle mixing state types

We calculated the margin of error (ME) corresponding to the number of the total particles measured at a 99% confidence interval. The equation is as follows,

$$\mathrm{N} = \frac{\mathrm{Z}^2 \times \mathrm{p} \times (1 - \mathrm{p})}{\mathrm{ME}^2} \qquad \text{Eq. S14}$$

where N is the number of the total particles (N = 197 in this study); Z is the z-value for a normal distribution (the corresponding Z value at a 99% confidence interval is 2.33); p is the proportion of each particle mixing state type.

Statistically, the proportion of individual particles with different mixing state types, namely, organic internally mixed with inorganic (OCIn), organic internally mixed with inorganic and soot (OCInEC), organic internally mixed with soot (OCEC), and pure organic (OC) was 73.1%, 20.8%, 4.1%, and 2.0%, respectively. Therefore, the corresponding ME is 7.4%, 6.7%, 3.3%, and 2.3%, respectively.

Figures

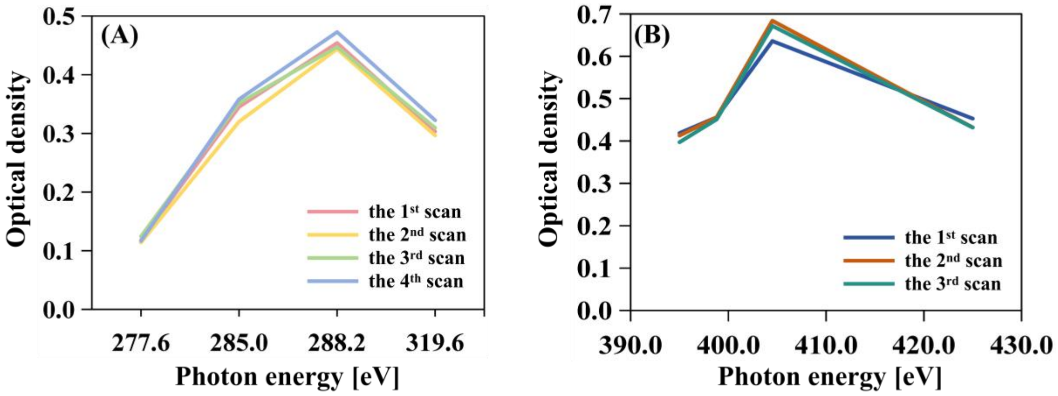

Figure S 1: Spectra collected over the same spot at different photon energies at the (A) carbon and (B) nitrogen K-edges.

As displayed in Fig. S1, optical density at different photon energies of several scans resembles each other at both the carbon and nitrogen K-edges, which indicates no obvious beam damage occurred.

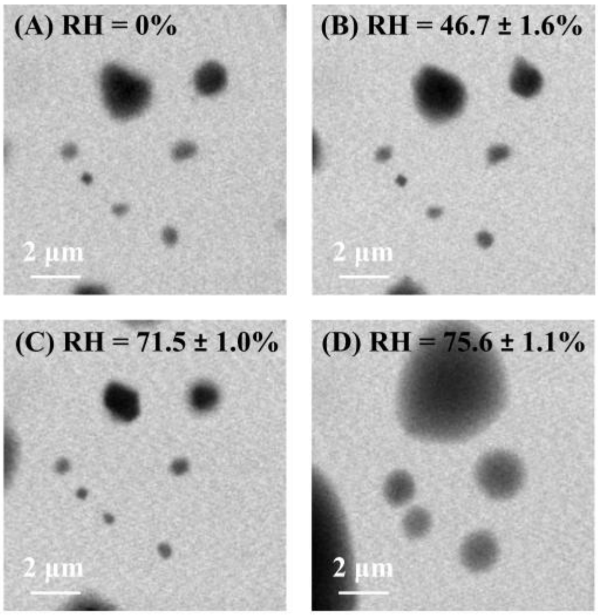

Figure S 2: Images of a sodium chloride (NaCl) standard sample at different relative humidity (RH): (A) RH = 0%, (B) RH = 46.7 ± 1.6%, (C) RH = 71.5 ± 1.0%, and (D) RH = 75.6 ± 1.1%. The images were gained at a photon energy of 550.0 eV. Uncertainty was estimated from the RH stability and sensor accuracy over hours.

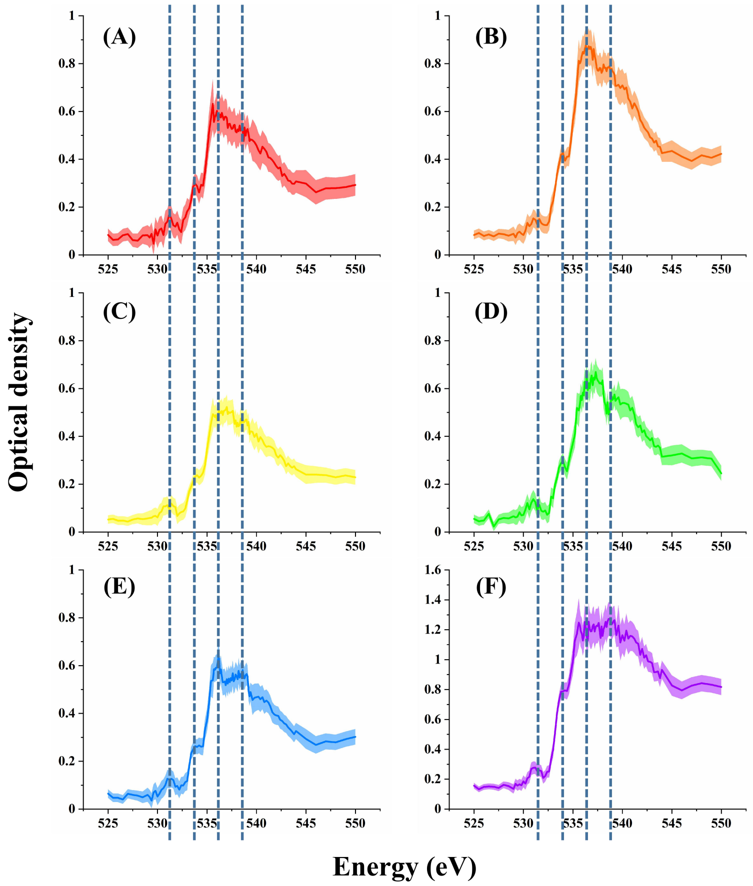

Figure S 3: Oxygen K-edge NEXAFS spectra of a NaCl standard sample at high RH. For panels (A) – (C), the RH was 75.6 ± 1.1%. For panels (D) – (F), the RH was 79.4 ± 0.8%. The upper and lower limits of shaded areas represent the optical density plus / minus one time of the standard deviation.

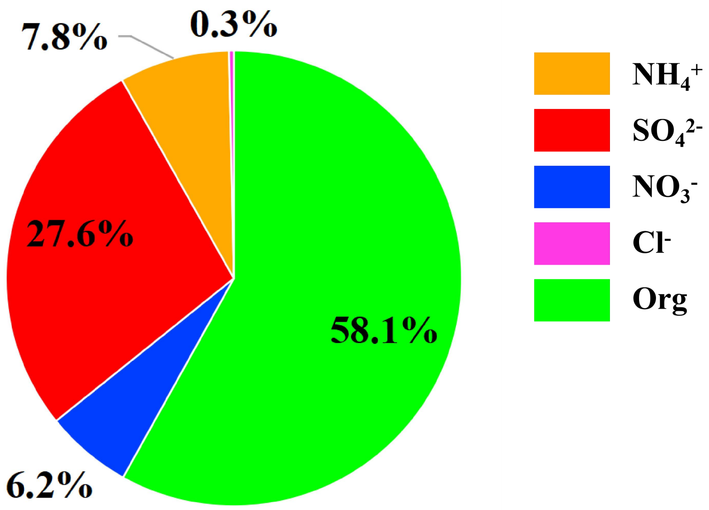

Figure S 4: Pie chart showing the average mass fractions of chemical composition of non-refractory submicron particles (NR-PM_1) during the sampling period of individual particles.

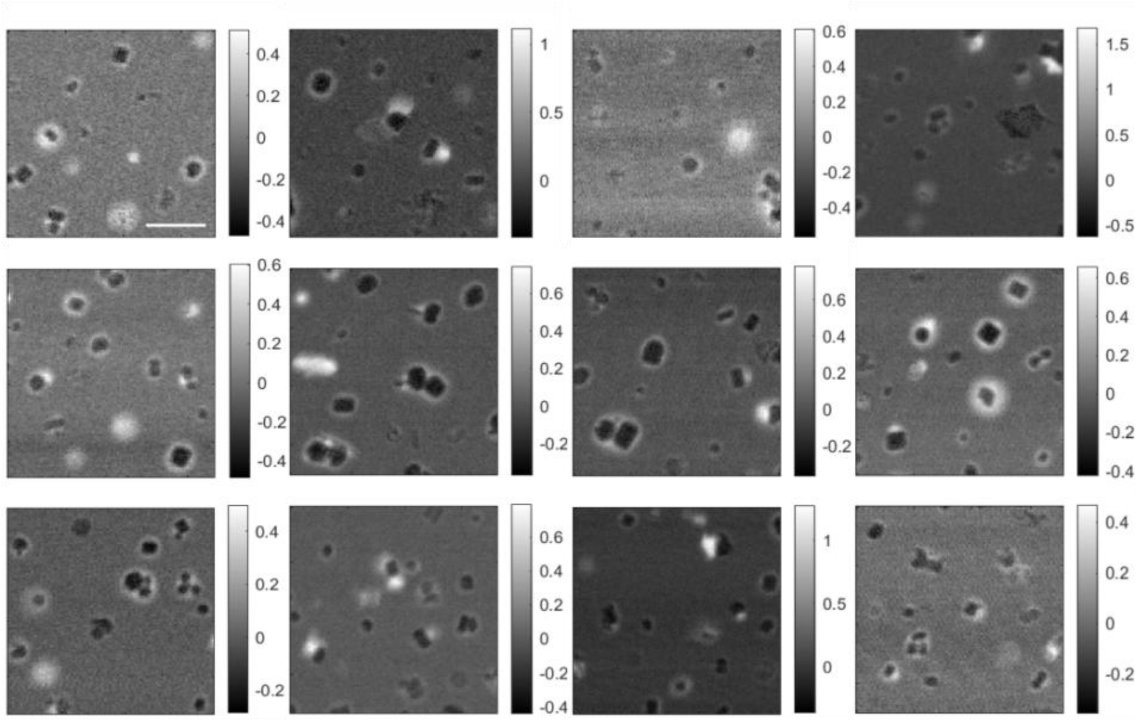

Figure S 5: Total carbon maps of particles under dry conditions, produced by subtracting the image at the pre-edge from that at the post-edge (OD_{320eV} - OD_{278eV}). The scale bar in white in the upper left image represents 2 μm and applies to all the images.

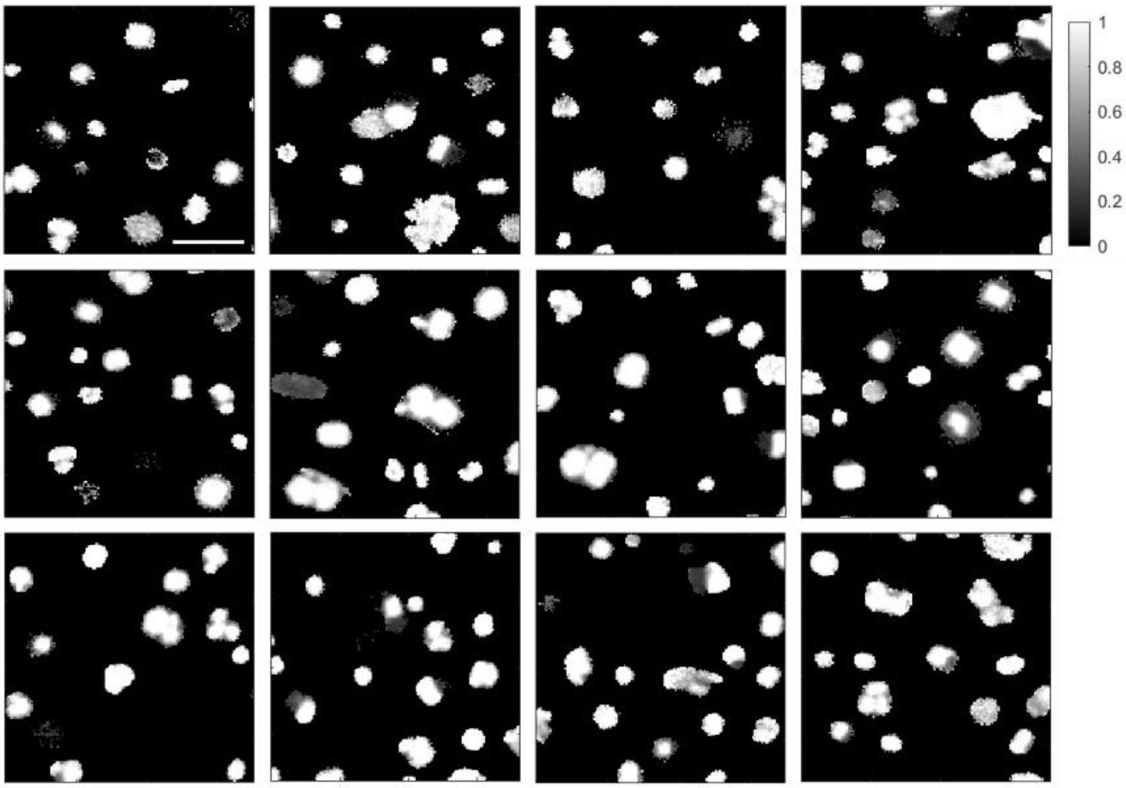

Figure S 6: Inorganic maps of particles under dry conditions, produced by taking the ratio of the image at the pre-edge to that at the post-edge (OD_{278eV} / OD_{320eV}). Scale bar in white in the upper left image represents 2 μm and applies to all the images.

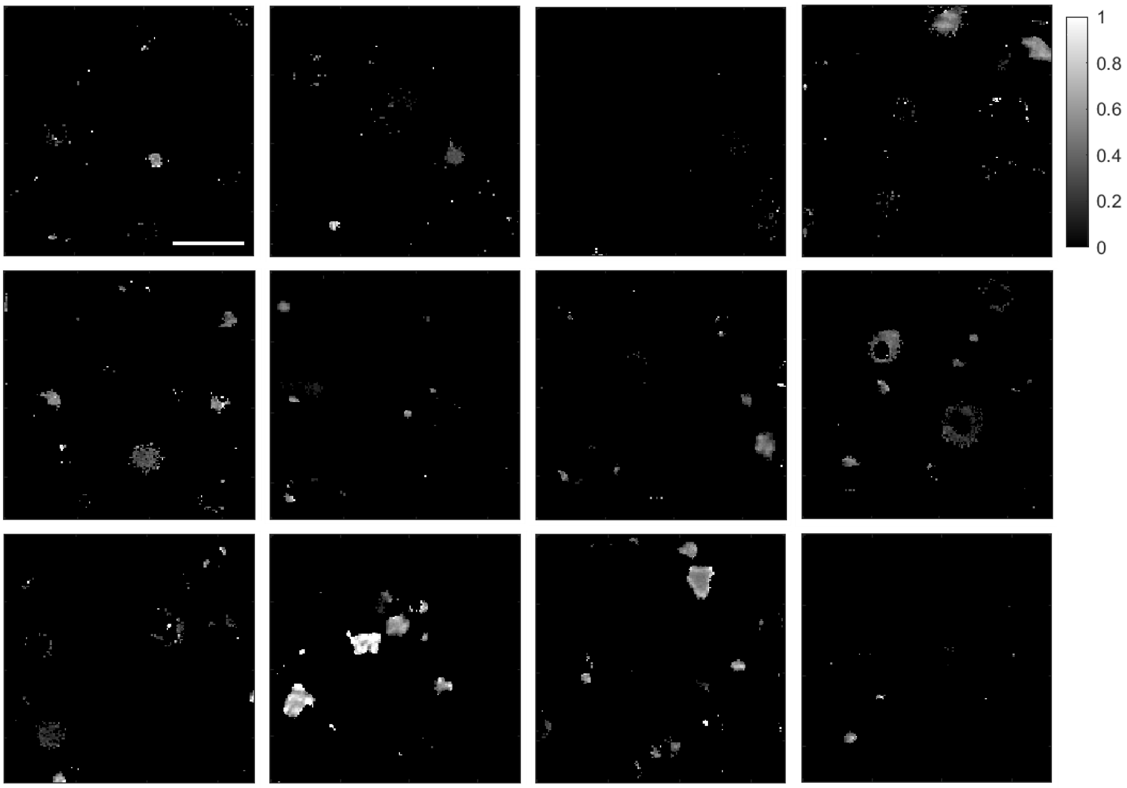

Figure S 7: sp^2 hybridized carbon maps of particles under dry conditions, calculated by the absorbance contribution of doubly bonded carbon to total carbon (%sp^2) in the highly oriented polycrystalline graphite. The scale bar in white in the upper left image represents 2 μm and applies to all the images.

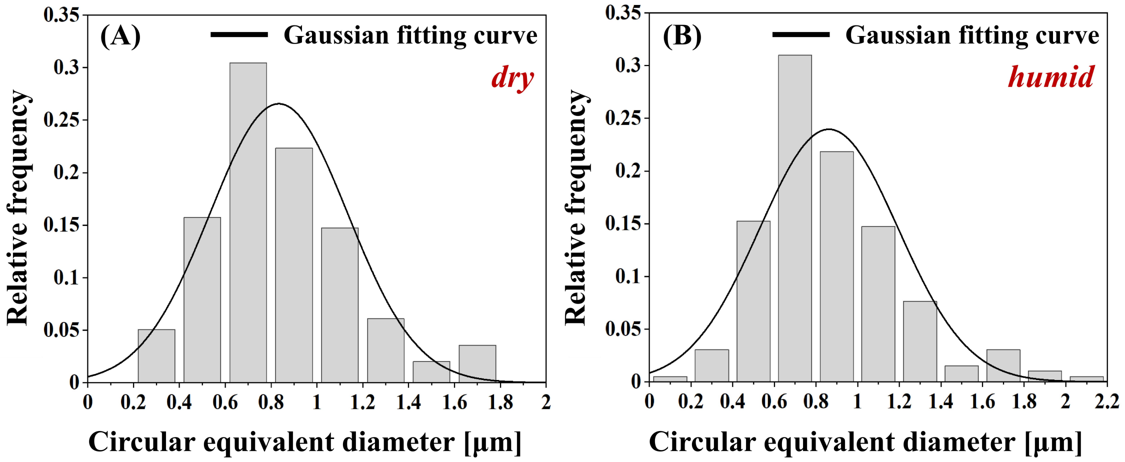

Figure S 8: The particle size distribution of the particle population under (A) dry and (B) humid conditions (RH = 86%). The black line represents the Gaussian fitting curve.

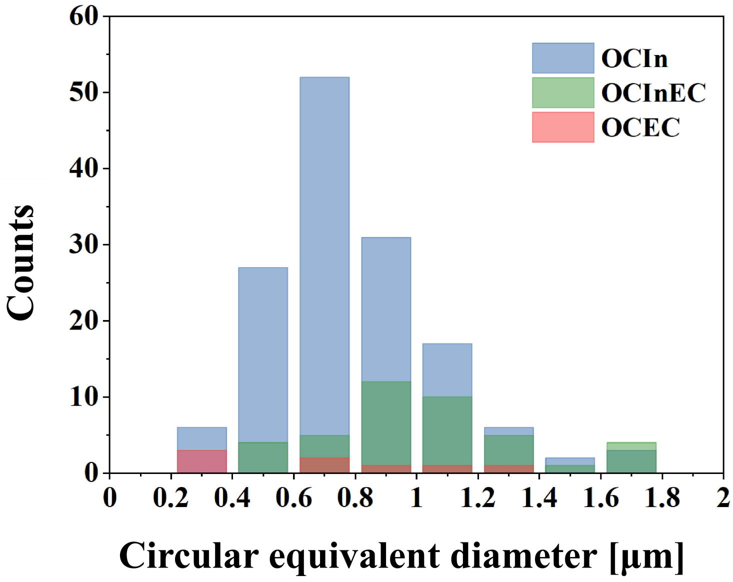

Figure S 9: Particle size distributions of three main mixing state types: organic internally mixed with inorganic (OCIn, displayed in blue), organic internally mixed with inorganic and elemental carbon (OCInEC, displayed in green), and organic internally mixed with soot (OCEC, displayed in red). Diameters here are the circular equivalent diameter in µm.

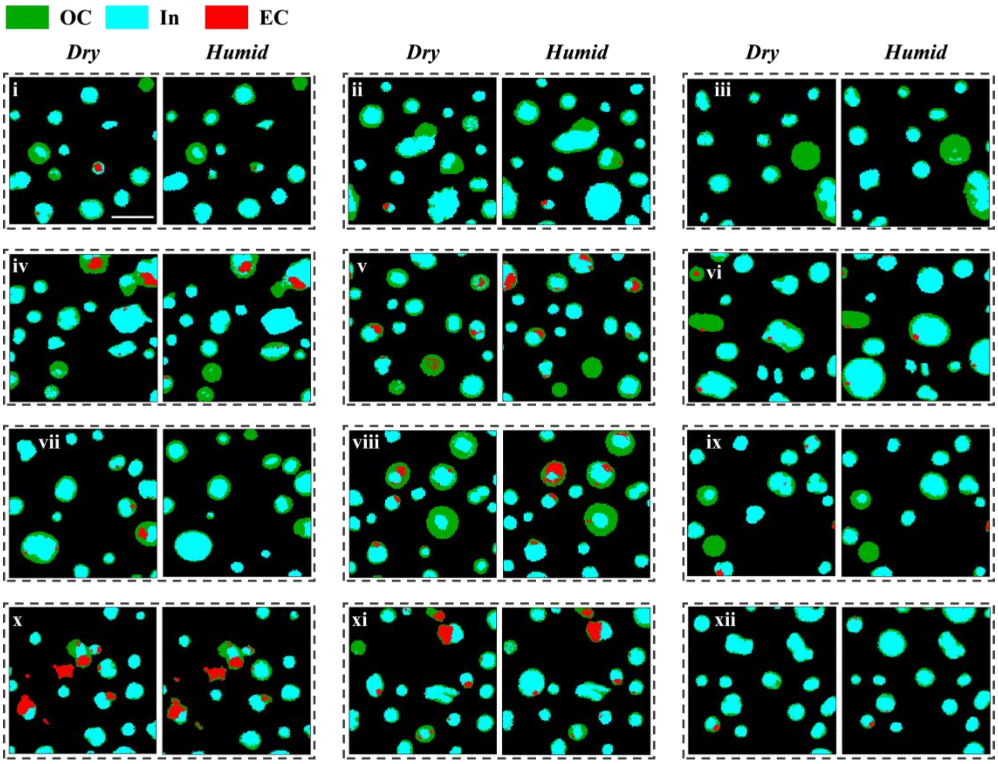

Figure S 10: Chemical maps of individual particles in 12 regions of interest under dry and humid conditions. Green, cyan, and red color represent dominant components of organic carbon (OC), inorganic matter (In), and elemental carbon (EC), respectively. The scale bar in the upper left image represents 2 μm and applies to all the images.

As shown in Fig. S11B, the main diameter range of particles that took up water (0.4 – 1.2 μm) was consistent with that of the overall particles. For submicron particles with diameters in the range of 0.2 – 0.8 μm, the fraction of hygroscopic particles decreased as size increased. Conversely, for particles with diameters in the range of 0.8 – 1.8 μm, the number fraction increased with size. Notably, the highest proportion of particles taking up water was observed in the smallest size range (0.2 – 0.4 μm, 80%), likely due to their chemical composition.

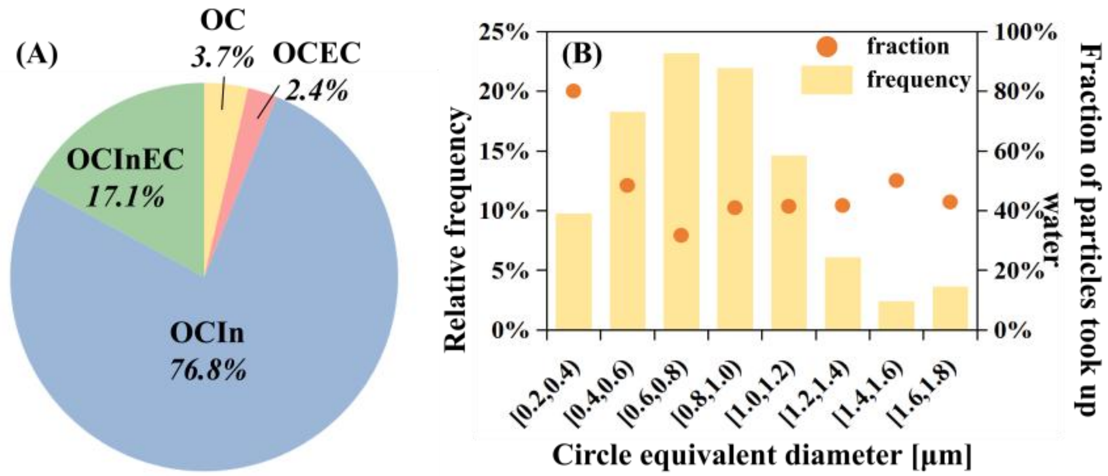

Figure S 11: (A) Proportions of the mixing state types of individual particles that took up water. Blue, green, yellow, and red represent particle mixing state types: OCIn, OCInEC, OC, and OCEC, respectively. (B) Relative frequency distribution of the particle size of particles taking up water (represented by light yellow columns), and the fraction of particles taking up water in each diameter range (represented by orange dots).

References

(1) Donahue, N. M.; Robinson, A. L.; Trump, E. R.; Riipinen, I.; Kroll, J. H. Volatility and aging of atmospheric organic aerosol. Atmospheric and Aerosol Chemistry; Springer Berlin Heidelberg, **2014**, pp 97-143. DOI: 10.1007/128_2012_355.

(2) Piens, D. S.; Kelly, S. T.; Harder, T. H.; Petters, M. D.; O'Brien, R. E.; Wang, B. B.; Teske, K.; Dowell, P.; Laskin, A.; Gilles, M. K. Measuring Mass-Based Hygroscopicity of Atmospheric Particles through in Situ Imaging. *Environmental Science & Technology.* **2016**, *50* (10), 5172-5180, Article. DOI: 10.1021/acs.est.6b00793.

(3) Cappa, C. D.; Smith, J. D.; Messer, B. M.; Cohen, R. C.; Saykally, R. J. The electronic structure of the hydrated proton: A comparative X-ray absorption study of aqueous HCl and NaCl solutions. *Journal of Physical Chemistry B.* **2006**, *110* (3), 1166-1171. DOI: 10.1021/jp0534582.

(4) Cappa, C. D.; Smith, J. D.; Wilson, K. R.; Messer, B. M.; Gilles, M. K.; Cohen, R. C.; Saykally, R. J. Effects of alkali metal halide salts on the hydrogen bond network of liquid water. *Journal of Physical Chemistry B.* **2005**, *109* (15), 7046-7052. DOI: 10.1021/jp0445324.

(5) Krepelová, A.; Huthwelker, T.; Bluhm, H.; Ammann, M. Surface Chemical Properties of Eutectic and Frozen NaCl Solutions Probed by XPS and NEXAFS. *Chemphyschem.* **2010**, *11* (18), 3859-3866. DOI: 10.1002/cphc.201000461.

(6) Sahle, C. J.; Gallerande, E. D.; Niskanen, J.; Longo, A.; Elbers, M.; Schroer, M. A.; Sternemann, C.; Jahn, S. Hydration in aqueous NaCl. *Physical Chemistry Chemical Physics.* **2022**, *24* (26), 16075-16084. DOI: 10.1039/d2cp00162d.

(7) Zelenay, V.; Huthwelker, T.; Krepelová, A.; Rudich, Y.; Ammann, M. Humidity driven nanoscale chemical separation in complex organic matter. *Environmental Chemistry.* **2011**, *8* (4), 450-460. DOI: 10.1071/en11047.

(8) Henke, B. L.; Gullikson, E. M.; Davis, J. C. X-ray interactions: photoabsorption, scattering, transmission, and reflection at E=50-30000 eV, Z=1-92. *Atomic Data and Nuclear Data Tables*. **1993**, *54* (2), 181-342.

(9) Canagaratna, M. R.; Jimenez, J. L.; Kroll, J. H.; Chen, Q.; Kessler, S. H.; Massoli, P.; Hildebrandt Ruiz, L.; Fortner, E.; Williams, L. R.; Wilson, K. R. Elemental ratio measurements of organic compounds using aerosol mass spectrometry: characterization, improved calibration, and implications. *Atmosphere Chemistry and Physics*. **2015**, *15*, 253-272. DOI: 10.5194/acp-15-253-2015.